PHYSICAL REVIEW A VOLUME 59, NUMBER 6 JUNE 1999

Population inversion between atomic inner-shell vacancy states created by electron-impact ionization and Coster-Kronig decay

D. Kim,[1,2] C. Tóth,[2] and C. P. J. Barty[2]
[1]*Pohang University of Science and Technology, Pohang 790-784, Republic of Korea*
[2]*University of California, San Diego, La Jolla, California 92093-0339*
(Received 22 December 1998)

Population dynamics of atomic inner-shell vacancy states are analyzed for the possibility of inversion in relation to keV x-ray laser schemes. Transitions between pairs of inner-shell vacancy states are considered in which the states are pumped via electron-impact inner-shell ionization by a femtosecond high-energy electron pulse. For appropriate atomic systems, transient inversion is predicted due to rapid lower state depopulation via Coster-Kronig decay. [S1050-2947(99)50206-0]

PACS number(s): 42.55.Vc, 32.80.Hd, 34.80.Gs, 52.25.Nr

Recent advances in 10-fs-range, high-peak-power lasers [1–3] have renewed interest in developing keV x-ray lasers based on inner-shell atomic transitions [4–11]. Other approaches to creating short-wavelength, coherent x-ray sources, such as high harmonic generation [12,13] and x-ray lasers based on the fast recombination of ions [14,15] also benefit from short pulse excitation. Inner-shell x-ray laser schemes up to now have utilized photoionization for pumping [4–16]. In the original scheme of Duguay and Rentzepis [16], the lower state of the lasing transition was the ground state of the first ion and could not decay. The idea of utilizing a decaying lower state to insure inversion was suggested by Stankevich [17], elaborated by Arecchi *et al.* [18] and Elton [19], and calculated in detail by Axelrod for *K*-shell transitions [20]. The technical barrier to overcome for the successful realization of these schemes is the development of a sufficiently fast and energetic x-ray pump source whose time scale is of the order of the lifetime of the keV lasing transitions, i.e., in the 10-fs range [4,11,20]. The lack of such a source has prevented the realization of these schemes. In addition to this, the intrinsic problem with this scheme is that the electrons produced in photoionization and subsequent Auger decay are both energetic enough to collisionally ionize neutral atoms and thereby produce the lower state (thereby destroying the inversion) and rapidly deplete the neutral-atom population. If it were possible to create an inner-shell population inversion via atomic processes involving electrons only, then photoionization pumped x-ray laser schemes based on the same transitions would be less sensitive to secondary electron collisional filling of the lower state, require less demanding x-ray pumping conditions, and result in inversions that could be maintained longer, compared to equivalent photo-inner-shell ionization pumping schemes for the $K\alpha$ transition. The development of ultrafast electron sources is advancing rapidly. Ultrafast, high-energy ($\sim$keV) electron sources have been generated by femtosecond high-power lasers via optical field ionization (OFI). Ultrafast electron pulses produced by OFI have already been used to collisionally pump an extreme ultraviolet (XUV) laser in Xe^{8+} [21], where the full width at half maximum (FWHM) of the electron pulse was a few tens of femtoseconds. OFI also has been used to generate cold electrons for another x-ray laser scheme based on fast recombination [14,15]. Even the generation of sub-10-fs electron pulses via acceleration by laser plasma waves has been pursued both in theory and experiment [22–24]. These sources can have a higher conversion efficiency from laser light to energetic electrons, compared to that from laser light to incoherent plasma x rays of approximately the same energy.

This paper investigates the population dynamics of atomic inner-shell vacancy states driven by atomic processes involving electrons only, and proposes the optimal x-ray lasing scheme that uses electron-impact inner-shell ionization for pumping. If an atom were to be collisionally ionized by an instantaneous or δ-function electron pulse, the initial relative populations of its subshell vacancies would be set by its relative electron-impact ionization cross sections. Since these cross sections, for all atoms, are larger for outer-shell ionization than for inner-shell ionization, there would be no population inversion between vacancies initially. The subsequent populations would be determined by the rate at which each vacancy state decays due to radiative and Auger transitions. The decay rates of the vacancy states that may undergo Coster-Kronig or super-Coster-Kronig decay can be significantly larger than those of the next deeper vacancy states, i.e., the potential upper state of a lasing transition [25]. As pointed out in Ref. [7], for selected states in numerous atomic systems in which the lower state decay is mediated by Coster-Kronig or super-Coster-Kronig decay while the upper state is not, a transient, femtosecond–time-scale inversion can be achieved. As mentioned above, photoionization pumped inner-shell x-ray laser schemes using these transitions will benefit from this concept because the additional rate out of the lower state can overcome secondary filling processes.

We have surveyed radiative and nonradiative (Auger and Coster-Kronig) decay rates from *K*-, *L*-, *M*-, and *N*-shell vacancies in elements up to $Z=90$ [25–28]. We have considered transitions (i) whose lower states have shorter lifetimes than the upper states, (ii) whose upper states still have reasonably small natural width (<1 eV), thus allowing a realistic time scale of pumping, (iii) that have strong fluorescence allowing large gain cross sections, and (iv) whose transition energies are in the keV range. These conditions are satisfied

TABLE I. Characteristics of inner-shell transitions in tested atoms. The decay rate is for the upper state. The $D(P)$ ratio is the ratio of decay (collisional ionization) rates of the lower state to that of the upper state. The inversion densities were calculated for the electron pulse with a duration of 10 fs FWHM and a maximum density of $10^{21}\,\mathrm{cm}^{-3}$.

Transition	Z range	Tested atoms (Z)	λ (nm)	Decay rate (fs^{-1})	D ratio	P ratio	N_{inv} ($10^{19}\,\mathrm{cm}^{-3}$)
$L_1 \rightarrow M_3$	52–75	Cs(55)	2.63	6.68	1.2	46	$<10^{-10}$
$L_2 \rightarrow M_1$	20–90	Ti(22)	3.09	0.37	13.5	11.8	1.1
$L_3 \rightarrow M_1$	20–90	Ti(22)	3.15	0.37	13.5	11.8	0.5
$L_3 \rightarrow N_5$	65–85	Er(68)	0.15	7.13	1.3	288	$<10^{-10}$
$M_4 \rightarrow N_2$	44–90	Sn(50)	3.10	0.79	28.5	26	0.012

by the $L_1 \rightarrow M_3$, $L_{2,3} \rightarrow M_1$, $L_3 \rightarrow N_5$, and $M_4 \rightarrow N_2$ transitions for a wide range of atoms listed in Table I, where $A \rightarrow B$ refers to a transition between a single-vacancy state in the A (sub)shell and one in the B (sub)shell. The gain cross sections of these transitions are of the order of 10^4–10^5 b, and therefore require population densities of the order of $10^{19}\,\mathrm{cm}^{-3}$ for the gain of a few cm^{-1}.

To study the population dynamics of relevant states among these transitions and thus allow determination of the ''best'' scheme among the many possibilities listed in Table I, we have numerically solved the following rate equations for the populations of the states of interest when neutral atoms are ionized by a short, intense electron pulse:

$$\frac{dN_2}{dt} = P_2 N_e N_0 - D_2 N_2, \tag{1}$$

$$\frac{dN_1}{dt} = P_1 N_e N_0 - D_1 N_1 + A_{21} N_2, \tag{2}$$

$$\frac{dN_0}{dt} = -P_{\mathrm{total}} N_e N_0. \tag{3}$$

The ground state of the neutral atom is the state 0, and the upper and lower states are the states 2 and 1, respectively. For each state k, N_k is the population; P_k the collisional ionization rate; D_k the total decay rate including radiative, Auger, and Coster-Kronig processes; A_{21} the radiative transition rate between the states 2 and 1; P_{total} the total collisional ionization rate summed over all the subshells; and N_e the time-dependent electron density. Photoionization processes were not included. The incident electron pump pulse is assumed to be monoenergetic and P_k is then given by $N_e\,\sigma v$, where σ and v are the collisional ionization cross section and velocity of electrons, respectively. The energy of the electron was chosen so that it maximizes the electron-impact inner-shell ionization of the shell whose vacancy state is the upper state. For instance, the binding energy of the L_2 subshell in Ti is 462 eV and the collisional ionization cross section of the subshell reaches its maximum at the energy that is ~6 times larger than the threshold energy [29]. Hence, for the simulation of the population dynamics of the $L_2 \rightarrow M_1$ transition in Ti, an electron energy of 2800 eV was used. This ensures the maximum pumping rate to the upper state. The FWHM of the Gaussian electron pulse was varied from 0.1 to 30 fs. For a few keV energy, electron-electron thermalization time is very long (a few tens of picoseconds), even at a density of $10^{21}\,\mathrm{cm}^{-3}$, and the initial electron energy distribution is still expected to be maintained for the time scale of our interest (i.e., less than 50 fs). Three-body recombination and dielectronic capture (inverse Auger) processes were neglected because they are very slow (on the order of a few tens to hundreds of microseconds) for the energy and density in this study. The simulation integrates the first-order rate equations forward in time with a first-order difference scheme and calculates the populations of the relevant states and the inversion density $N_{\mathrm{inv}} = N_2 - (g_2/g_1)N_1$, where g_k is the statistical weight of the state k. The un-ionized laser material was initially set to be cold (no free electrons) and at normal solid density and allowed to be depleted at the total ionization rate (summed over all the subshells) as the inner-shell ionization was taking place.

Figure 1 shows the change of the populations of the upper and lower states and the inversion density for the case of Ti. $T=0$ is the time when the 10-fs electron pulse reaches its maximum. Due to the higher ionization rate to the lower state, no inversion initially takes place, but the faster decay of the lower state allows the inversion to take place later in time around the peak of the electron pulse. The inversion lasts about 15 fs. Table I shows the simulation results for the best candidate atom for each scheme. Comparison is made with the electron ionization pulse of 10-fs FWHM and the maximum density of $10^{21}\,\mathrm{cm}^{-3}$. The most important factors

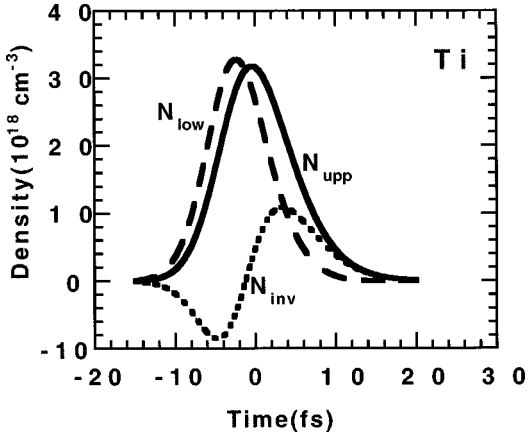

FIG. 1. Change of the populations and inversion density for the case of Ti, calculated with the electron pulse with a duration of 10 fs FWHM and a maximum density of $10^{21}\,\mathrm{cm}^{-3}$.

for achieving high inversions are the ratio of the decay rate from the lower state to that from the upper states (D ratio $=D_1/D_2$) and the ratio of the collisional pumping rate to the lower state to that to the upper states (P ratio$=P_1/P_2$). While inversions were observed when the P ratio was comparable to the D ratio, no inversion was achieved when the P ratio was larger than the D ratio. It is interesting to note that a smaller P ratio produces higher inversion than a larger D ratio (the $L_3 \rightarrow M_1$ transition in Ti vs the $M_4 \rightarrow N_2$ transition in Sn). The $L_2 \rightarrow M_1$ transition has higher inversion than the $L_3 \rightarrow M_1$ transition, due to its favorable degeneracy.

Among these transitions, the $L_2 \rightarrow M_1$ transition in atoms for Z equal to or higher than 20 appears to have the least stringent requirements. Calcium is the first element in which the M_1 shell decays rapidly via an $M \rightarrow MN$ Coster-Kronig transition. Figure 2(a) shows the inversion characteristics of this $L_2 \rightarrow M_1$ transition in several low-Z atoms. For these calculations the total number of electrons integrated over the pulse duration was fixed in such a way that the maximum electron density was $10^{21}\,\mathrm{cm}^{-3}$ for a 10-fs FWHM electron pulse. As expected, the shorter the pump pulse, the higher the inversion density. However, the marginal increase of inversion density from the 1-fs to the 0.1-fs pumping case is smaller than that from the 10-fs to the 1-fs pumping. This is because the collisional ionization rate for 1-fs pumping at the maximum electron density of $10^{22}\,\mathrm{cm}^{-3}$ becomes enough to deplete significantly the neutral-atom population. Shorter duration pumping becomes beneficial only if electron density is decreased, but in this case the magnitude of the inversion density becomes less also. The highest degree of inversion was obtained for titanium. This is due to the delicate balance between the decay rates of the upper and the lower states. Calcium and scandium have smaller inversion density because the decay rate of the lower state is two or three times slower than that in titanium, while the decay rates of the upper states of calcium and scandium are slightly slower than that in titanium. Titanium has two *3d* electrons that enhance the decay from the single vacancy state in the M shell through the super-Coster-Kronig process. As shown in Fig. 2(b), the gain is largest for scandium for pumping with a 10-fs electron pulse, while the degree of the inversion is still largest in titanium. This is due to scandium's larger gain cross section. Higher Z atoms than titanium have smaller inversion density because their upper states decay faster and the ratios of the decay rates from the upper states and the lower states become more unfavorable for inversion. Since the gain cross section is smaller for higher-Z atoms [open square in Fig. 2(b)], gains for higher-Z atoms were always smaller than titanium, regardless of the pumping duration.

Such calculations predict that small signal gains of $3.9\,\mathrm{cm}^{-1}$ at 3.52 nm (353 eV) in Sc, $3.8\,\mathrm{cm}^{-1}$ at 3.09 nm (401 eV) in Ti, and $1.3\,\mathrm{cm}^{-1}$ at 2.44 nm (509 eV) in Cr could be achieved for an electron pulse of 10-fs FWHM with the energy of 2.4 keV (for Sc), 2.8 keV (for Ti), and 3.5 keV (for Cr), and a maximum electron density of $10^{21}\,\mathrm{cm}^{-3}$. Shorter duration electron pulses will produce higher gain, as illustrated in Fig. 2(b). Even though the interaction of high-field femtosecond laser pulses with matter and plasma is under active investigation, reliable values for the conversion efficiency of laser energy into high-energy electrons are sparse. An estimate of the energy of the pump electron beam

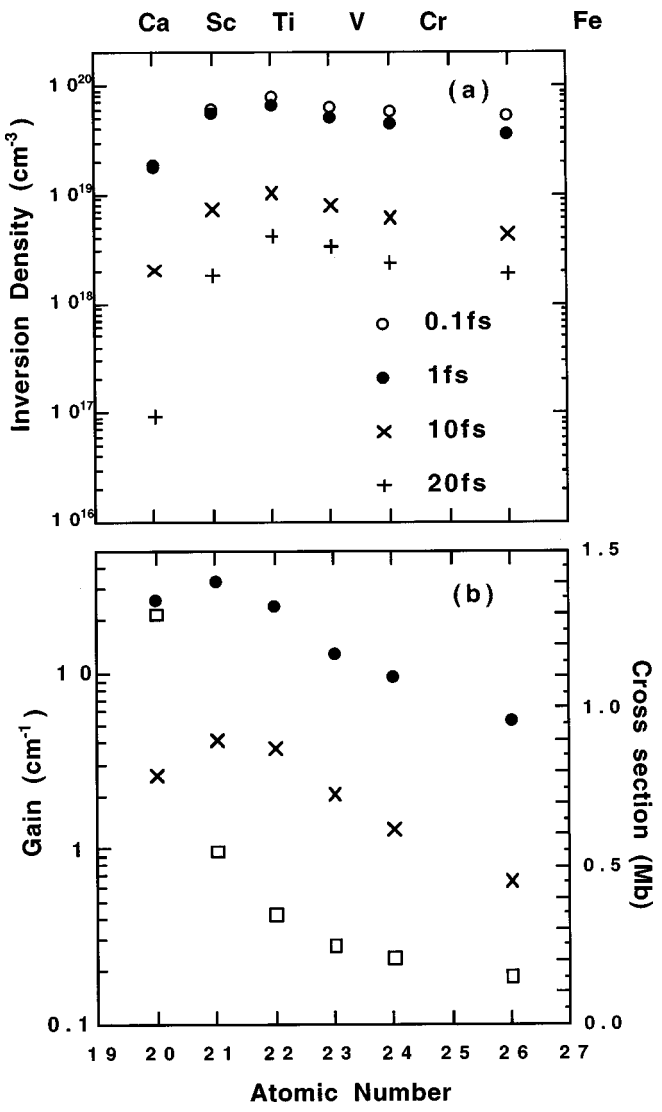

FIG. 2. Change of the inversion density of the $L_2 \rightarrow M_1$ transition with respect to elements and the duration (FHWM) of driving electron pulses. (b) Gain characteristics of the $L_2 \rightarrow M_1$ transition with respect to elements calculated with the electron pulse with a duration of 10 fs FWHM (crosses) and 1 fs FWHM (solid circles) and a maximum density of 10^{21} and $10^{22}\,\mathrm{cm}^{-3}$, respectively. The change of the gain cross section of the $L_2 \rightarrow M_1$ transition (open squares) is also shown.

is still useful to set a lower bound for the pump energy required to achieve inversion. For the case of Ti, electrons of $\sim$3 keV are necessary. Considering an illuminated area of 10 μm $\times$ 2 cm, an inversion of $10^{19}\,\mathrm{cm}^{-3}$ requires a total energy of the electron beam at a density of $10^{21}\,\mathrm{cm}^{-3}$ of 5 mJ.

In conclusion, by investigating the population dynamics of inner-shell transitions for various elements up to $Z=90$, we have demonstrated that there exist inner-shell transitions in which inversion of relevant states can be achieved even with atomic processes involving only electrons. Furthermore, we have determined the best scheme for inversion of a different class of x-ray laser in which the upper state is pumped by electron inner-shell ionization. The $L_2 \rightarrow M_1$ transition is most feasible for atoms between $Z=20$ and $Z=28$.

For pumping durations up to 30-fs FWHM, the highest

inversion is expected in titanium. The application of these transitions to photoionization pumped schemes would lead to less demanding incoherent x-ray pumping requirements and longer gain durations. Detailed further study in this direction is in progress.

Dong-Eon Kim is on sabbatical leave at the University of California, San Diego, and is grateful for the support from the Wilson group at UCSD, the Seo-Ahm Scholarship Foundation, and the Basic Science Research Institute (Grant No. BSRI98-2439).

[1] K. Yamakawa, M. Aoyama, S. Matsuoka, H. Takuma, C. P. J. Barty, and D. Fittinghoff, Opt. Lett. **23**, 525 (1998).
[2] C. P. J. Barty, T. Guo, C. Le Blanc, F. Raksi, C. Rose-Petruck, J. Squire, K. R. Wilson, V. V. Yakovlev, and K. Yamakawa, Opt. Lett. **21**, 668 (1996).
[3] J. P. Chambaret, C. Le Blanc, G. Cheriaux, P. Curley, G. Darpentigny, P. Rousseau, G. Hamoniaux, A. Antonetti, and F. Salin, Opt. Lett. **21**, 1921 (1996).
[4] S. J. Moon and D. C. Eder, Phys. Rev. A **57**, 1391 (1998).
[5] K. Moribayashi, A. Sasaki, and T. Tajima, Phys. Rev. A **58**, 2007 (1998).
[6] Y. Li, H. Schillinger, C. Ziener, R. Sauerbrey, Opt. Commun. **144**, 118 (1997).
[7] C. P. J. Barty, T. Guo, C. Le Blanc, F. Ráksi, C. Rose-Petruck, J. Squier, B. C. Walker, K. R. Wilson, V. V. Yakovlev, and K. Yamakawa, Inst. Phys. Conf. Ser. **151**, 282 (1996).
[8] D. L. Matthews, Inst. Phys. Conf. Ser. **151**, 32 (1996).
[9] S. Meyer, T. Menzel, B. Wellegehausen, P.-X. Lu, S. Insam, and E. Fill, Inst. Phys. Conf. Ser. **151**, 173 (1996).
[10] G. L. Strobel, R. A. London, and D. C. Eder, Appl. Phys. B: Lasers Opt. **60**, 513 (1995).
[11] H. Kapteyn, Appl. Opt. **31**, 4931 (1992).
[12] M. Schnürer, Ch. Spielmann, P. Wobrauschek, C. Streli, N. H. Burnett, C. Kan, K. Ferencz, R. Koppitsch, Z. Cheng, T. Brabec, and F. Krausz, Phys. Rev. Lett. **80**, 3236 (1998).
[13] A. Rundquist, C. G. Durfee III, Z. Chang, C. Herne, S. Backus, M. M. Murname, and H. C. Kapteyn, Science **280**, 1412 (1998).
[14] Y. Nagata, K. Midorikawa, S. Kubodera, M. Obara, H. Tashiro, and K. Toyoda, Phys. Rev. Lett. **71**, 3774 (1993).
[15] D. V. Korobkin, C. H. Nam, S. Suckewer, and A. Goltsov, Phys. Rev. Lett. **77**, 5206 (1996).
[16] A. Duguay and P. M. Rentzepis, Appl. Phys. Lett. **10**, 350 (1967).
[17] Y. L. Stankevich, Dokl. Akad. Nauk [Sov. Phys. Dokl. **15**, 356 (1970)].
[18] F. T. Arecchi, G. P. B. Banfi, and A. M. Malvezzi, Opt. Commun. **10**, 214 (1974).
[19] R. C. Elton, Appl. Opt. **14**, 2243 (1975).
[20] T. S. Axelrod, Phys. Rev. A **13**, 376 (1976).
[21] B. E. Lemoff, G. Y. Yin, C. L. Gordon III, C. P. J. Barty, and S. E. Harris, Phys. Rev. Lett. **74**, 1574 (1995).
[22] S.-Y. Chen, R. Wagner, A. Maksimchuk, and D. Umstadter, in *Ultrafast Phenomena XI*, edited by T. Elsässer, J. G. Fujimoto, D. A. Wiersma, and W. Zinth, Springer Series in Chemical Physics Vol. 63 (Springer-Verlag, Berlin, 1998), p. 418.
[23] D. Umstadter, J. K. Kim, and E. Dodd, Phys. Rev. Lett. **76**, 2073 (1996).
[24] K. Nagashima, Y. Kishimoto, and H. Takuma, Phys. Rev. E **59**, 1263 (1999).
[25] M. O. Krause, J. Phys. Chem. Ref. Data **8**, 307 (1979).
[26] E. J. McGuire, Phys. Rev. A **3**, 587 (1971).
[27] E. J. McGuire, Phys. Rev. A **5**, 1052 (1972).
[28] J. H. Scofield, At. Data Nucl. Data Tables **14**, 121 (1974).
[29] W. Lotz, Z. Phys. **206**, 205 (1967); V. M. Pessa and W. R. Newell, Phys. Scr. **3**, 165 (1971).